JAERI-M
87-209

NEUTRAL BEAM CURRENT DRIVE FOR INTOR: THE POTENTIAL IN STEADY STATE AND QUASI STEADY STATE OPERATIONS

January 1988

Kunihiko OKANO,* Shin YAMAMOTO
Masayoshi SUGIHARA and Noboru FUJISAWA

日 本 原 子 力 研 究 所
Japan Atomic Energy Research Institute

JAERI-Mレポートは，日本原子力研究所が不定期に公刊している研究報告書です。
入手の問合わせは，日本原子力研究所技術情報部情報資料課（〒319－11茨城県那珂郡東海村）あて，お申しこしください。なお，このほかに財団法人原子力弘済会資料センター（〒319-11茨城県那珂郡東海村日本原子力研究所内）で複写による実費頒布をおこなっております。

JAERI-M reports are issued irregularly.
Inquiries about availability of the reports should be addressed to Information Division, Department of Technical Information, Japan Atomic Energy Research Institute, Tokai-mura, Naka-gun, Ibaraki-ken 319-11, Japan.

編集兼発行　日本原子力研究所
印　　刷　日立高速印刷株式会社

JAERI-M 87-209

NEUTRAL BEAM CURRENT DRIVE FOR INTOR: THE POTENTIAL IN STEADY STATE AND QUASI STEADY STATE OPERATIONS

Kunihiko OKANO*, Shin YAMAMOTO
Masayoshi SUGIHARA and Noboru FUJISAWA

Department of Large Tokamak Research
Naka Fusion Research Establishment
Japan Atomic Energy Research Institute
Naka-machi, Ibaraki-ken, Japan

(Received December 12, 1987)

The neutral beam current drive potential was investigated for INTOR benchmark test parameters. Various parameter dependences for the current drive efficiency were calculated and the 500 keV beam feasibility in INTOR design was clarified. The calculation includes spatial distributions for the beam driven currents. A flexible current profile control ability has been confirmed. It was also revealed that the same beam system could be used for strict steady state operation and for transformer recharging in quasi-steady state scenarios.

Keywords: Neutral Beam, Current Drive, INTOR, Current Profile Control, Transformer Recharge, Steady State Operation

---

* Toshiba Research and Development Center

INTOR用中性粒子電流駆動
定常と準定常運転の可能性

日本原子力研究所那珂研究所臨界プラズマ研究部
岡野　邦彦*・山本　　新・杉原　正芳・藤沢　　登

（1987 年12月12日受理）

国際協力で設計が進められている次期核融合実験装置 INTOR における，中性粒子入射電流駆動法の可能性とその性能を，INTOR ベンチマークテストパラメータを使って調べた。電流駆動効率の様々なパラメータ依存性を計算し，500 KeV ビームの INTOR 設計における可能性を明らかにしている。ビーム駆動電流の空間分布についても計算した。その結果，フレキシブルな電流分布制御性が確かめられた。また，完全定常運転用のビーム・システムは，そのまま準定常運転のトランスフォーマー再充電時用としても利用できることも明らかになった。

那珂研究所：〒 311-02 茨城県那珂郡那阿町大字向山 801-1
＊（株）東芝　総合研究所

Contents

目　　次

1. Introduction

A non-inductive current-drive would be one indispensable technology to make the tokamak system a more attractive reactor candidate. Although lower hybrid wave current-drive is most successful to date, the recent beam current drive experiments in JET [11] and TFTR [12], where over half mega ampere currents have been driven, imply the large potential for the NBI (neutral beam injection) current drive method.

This report presents results of investigations on the beam current driver potential for the next generation tokamaks. The feasibility of sub MeV beams is mainly discussed, because of ambiguity in regard to the near future development of over 1 MeV beams, while about 1.5 MeV beam will give the best current drive efficiency for the next generation tokamaks.

2. Beam Current Drive Model

2.1 Beam Current Drive Theory

After the first proposal of beam current drive by Ohkawa [1], the 2-D Fokker Planck equation has been used to investigate the beam current drive.

The velocity distribution for the fast ions, $f_b(v,\xi)$, generated by a neutral beam injection, is described by the Fokker-Planck equation. With the Legendre polynomial P_ℓ, the solution for f_b is written in an integration form [2,3]:

$$f_b(v,\xi) = g_{cx}(v)\left[\frac{S_0\tau_{se}}{v^3+v_c^3}\sum_{\ell=0}^{\infty}\frac{2\ell+1}{2}P_\ell(\xi_b)P_\ell(\xi)\left\{\frac{v^3}{v_c^3}\,\frac{v_b^3+v_c^3}{v^3+v_c^3}\right\}^{\frac{1}{6}\ell(\ell+1)Z_2}U(v_b-v)\right] \quad (1)$$

where $U(v_b - v)$ is the Heaviside step function and $\xi = \cos\theta$ is the pitch angle for fast ions along the magnetic field, S_0 is the particle source at (v_b,ξ_b) due to the injection, τ_{se} and v_c are the slowing down time due to the electrons and the critical velocity where the energy loss rate for fast ions to electrons and to ions is equal. Assuming $\log \Lambda_i = 24$ and $\log \Lambda_e = 17$, these values are reduced as follows:

$$\tau_{se} = 1.17 \times 10^{18}\ A_b\ (T_e/\mathrm{keV})^{3/2} / (Z_b^2 n_e)\ \ [\mathrm{sec}] \quad (2)$$

$$v_c = 1.42 \times 10^{6}\ (T_e/\mathrm{keV})^{1/2}\ \ [\mathrm{m/sec}] \quad (3)$$

where A_b and Z_b are the mass number and the charge number for the fast ions, and

$$Z_2 = (\sum_i \log \Lambda_i n_i Z_i^2/A_b) \,/\, (\sum_i \log \Lambda_i n_i Z_i^2/A_i) \quad . \tag{4}$$

The function $g_{cx}(v)$ is a particle loss factor due to charge exchange [3]. When the charge exchange fast ion loss is negligible, $g_{cx}(v)$ is unity.

Using f_b in Eq. (1), ion current density j_i, driven by the neutral beam injection, is given by

$$j_i = eZ_b \int_0^\infty v^3 dv \int_{-1}^{1} f_b(v,\xi)\,\xi d\xi \quad . \tag{5}$$

The orthogonality of the P_n has reduced the sum over n to the n = 1 term [9]. Then, Eq. (5) reduces to

$$j_i = eZ_b S_0 \tau_{se} \xi_b v_0 \frac{1}{x_b} \left(\frac{x_b^3+1}{x_b}\right)^y \int_0^{x_b} g_{cx}(x) \left(\frac{x^3}{x^3+1}\right)^{y+1} dx \quad , \tag{6}$$

where $y = Z_2/3$, which is a parameter on the pitch angle diffusion. Total driven current j_t is a sum of the fast ion current and a back streaming electron current induced due to the momentum transfer to the electrons from the fast ions. Therefore, current drive efficiency, by neutral beam injection, is

$$\frac{j_t}{p_b} = \frac{2eZ_b \tau_{se} \xi_b}{m_p A_b v_c} J(x_b,y)\,[1 - Z_b/Z_{eff}\{1 - G(Z_{eff},\varepsilon)\}] \tag{7}$$

$$J(x_b,y) = \frac{1}{x_b^2} \left(\frac{x_b^3+1}{x_b}\right)^y \int_0^{x_b} g_{cx}(x) \left(\frac{x^3}{x^3+1}\right)^{y+1} dx \quad , \tag{8}$$

where the final term in Eq. (7) shows the reduction in driven current, due to the back streaming electrons, ε is inverse aspect ratio and factor G (order of unity) has been calculated by Start et al. [8]. For example, when $Z_{eff} = 2$ and $\varepsilon = 0.2$, $G = 0.84$. Functional approximations for G and J, without charge exchange loss, are found in Ref. [9]. Functions $g_{cx}(v)$ and J, with charge exchange loss, are found in Ref. [3].

2.2 Beam Penetration and Shinethrough

The neutral beams traversed through the toroidal field must be re-ionized in the plasma. This re-ionization occurs by various atomic processes. The cross-sections of three important processes, electron impact ionization σ_e, proton impact ionization σ_p and charge exchange σ_x, are shown in Fig. 1, where σ_e is the Maxwellian average, i.e., $\sigma_e = \langle\sigma v\rangle_e / v_0$ (v_0 is the injection speed) [4]. The total effective ionization cross section is defined by

$$\sigma_{eff} = \{n_e\sigma_e + (\sigma_p + \sigma_x) \sum_i n_i\} / n_e \quad . \tag{9}$$

In the case of over 100 keV injection, the charge exchange process is negligible. Also the authors have neglected the impurity impact ionization in Eq. (9), while the beam current drive analysis code includes it. The shinethrough fraction of beam power, f_s, is

$$f_s = \exp(-\tau)$$

where τ, the number of ionization mean free paths traversed through the plasma, is given by

$$\tau = \int_{-L}^{L} n_e(r)\sigma_{eff}(r)ds \quad ,$$

where L is half length of the beam path (s) in the plasma. For example, $\tau = 3$ gives about 5 % shinethrough. A too large τ (>> 5) causes surface heating and a low τ (<< 2) results in too much shinethrough. Figure 2 shows an example of beam power deposition profile function H(r) for various τ. The deposition power density (Watts/m^3) is given by $P_b H(r)/2\pi R$, where P_b is the injection power, R is the plasma major radius. In this example, 500 keV beam energy and the parameters (R = 5.2 m, a = 1.12 m, κ = 1.6, R_{tang} = 4.6 m) are assumed with a rectangular beam line cross-section of 1.2 m (in height) x 0.4 m (in width).

2.3 Beam Current Drive Analysis Code

In order to investigate the beam-driven currents and the driver powers, the authors have developed an up-graded version of the beam current drive analysis code used in Ref. [5]. The new version consists of a 2-D current profile calculation code and a 3-D beam power and momentum deposition code. In both codes, magnetic flux surfaces, labeled by ψ, are given by

$$R - (R_0 + \Delta_\psi) = r_\psi(\cos\theta - \delta_\psi|\sin\theta|) \qquad (10)$$

$$z = \pm\kappa_\psi r_\psi\sqrt{|\sin\theta|} \quad , \qquad (11)$$

where ψ is a poloidal flux function, r_ψ is a half width of the magnetic flux surface on the $z = 0$ plane, R_0 is major radius of torus and θ is poloidal angle, measured from the horizontal plane. Plasma elongation κ_ψ, triangularity $\delta_\psi (\equiv d)$ and r_ψ $(=a)$ at the plasma surface are given, which characterize the plasma shape. When discussing in detail the current profile consistent with the MHD pressure balance, the shape of each magnetic surface in the plasma and the axis shift for each magnetic surface Δ_ψ must be determined by an MHD equilibrium analysis. Such a full treatment on the beam driven MHD equilibria is deferred elsewhere. In this report, the authors chose rather κ_ψ, δ_ψ and Δ_ψ somewhat arbitrarily, except these values on the plasma surface, because the detailed forms of magnetic surfaces inside the plasma have a comparably small effect on the global current drive efficiency. These values, κ, δ and Δ, on the plasma surface are very important.

The beam power deposition calculation gives the portion of beam powers absorbed on each magnetic surface P_{dep}. Then it is converted in power density p_d, averaged on the flux surface, followed by

$$P_{dep}(\psi)d\psi = p_d(\psi)(dS_\psi/d\psi)2\pi\langle R\rangle_\psi, \tag{12}$$

where S_ψ is area of poloidal cross-section of the plasma inside the flux surface labeled by ψ. Average radius $\langle R\rangle_\psi$ is defined so that $2\pi\langle R\rangle_\psi S_\psi$ may give the volume surrounded by the flux surface ψ.

Toroidal ion current density by circulating fast ions, j_i, is derived from the velocity distribution of fast ions $f_b(\vec{v})$, as described by Eq. (1). In order to take into account fast ions energy diffusion, an ion distribution tail in a regime $v \geq v_b$ is added to $f_b(\vec{v})$;

$$f_{tail} = f_b(\vec{v}_b) + (\partial f/\partial \vec{v})_{v_b} \cdot (v - v_b) \quad , \tag{13}$$

where $(\partial f/\partial \vec{v})$ is determined by the manner in Ref. [2]. Nevertheless, the energy diffusion effect in the driven currents is always small (less than 5 %).

As $f_b(\vec{v})$ has been given by a linearized fast ion Fokker-Planck equation, the current-drive efficiency j_t/p_d has no dependence on power density p_d. Then, once j_i, driven by a unit power density, is obtained, j_t/p_d is known.

The p_d and j_t/p_d calculations are carried out on each magnetic surface, whereby the current-profile in the plasmas is known. Total driven current I_p is obtained by an integration of local current density $j_t(\psi) = (j_t/p_d)_\psi p_d(\psi)$;

$$I_p = \int j_t(\psi)(dS_\psi/d\psi)d\psi \quad . \tag{14}$$

Using I_p and injected beam power P_b, global current-drive efficiency I/P (= I_p/P_b) is determined. Note that P_b includes the shinethrough power, i.e. the power absorbed by the plasma is given by

$$P_{abs} = P_b(1 - f_s) \quad ,$$

where f_s is the shinethrough fraction of the beam power. Therefore, efficiency I/P depends on f_s. Calculating the beam power deposition profile and the shinethrough fraction is accomplished with a three dimensional model, where any beam line orientations (see Fig. 3), any profiles for the beam line cross-section and any shapes of the target plasmas (Dee, Bean etc.) can be treated. The code includes the cross-section data for ionizations and charge-exchanges due to the electrons, the fuel ions and various impurity ions [6,7].

The temperature and density distributions are assumed as in the following profiles;

$$T = T_0[1 - (r/a)^2]^{\alpha T}, \quad n = n_0[1 - (r/a)^2]^{\alpha n} .$$

The code also outputs the fusion power and the net electric output, where 'net' means (total electric output)-(electric power due to driver). These values strongly depend on the temperature and density profiles. The fusion power calculation includes a power from a beam-plasma direct reaction.

3. Current Drive Efficiency

3.1 Dependence on T_e and n_e

Figure of merit on global current drive efficiency

$$\gamma = \frac{I_p(MA)\bar{n}_e(10^{20}m^{-3})R(m)}{P_b(MW)}$$

depends on the plasma electron temperature $\bar{T}_e$. Also γ has a dependence on density $\bar{n}_e$, because of beam deposition characteristic change.

The beam driven currents are calculated by the beam current drive analysis code with the INTOR parameters (Parameters A) listed in Table 1. The magnetic flux surfaces used here are shown in Fig. 14. The beam parameters are listed in Table 3. The injection energy 500 keV is lower than the optimum energy ($\sim$ 1.5 MeV), which gives a maximum current drive efficiency, but it is more realistic for the INTOR design, when considering near future developments in beam technology [10]. The beam line is split into 16 beams in the beam current drive analysis code, as shown in Table 3, assuming a symmetry with respect to the tokamak equatorial plane. The actual calculation is done with the upper 8 beams only. (In the beam power deposition calculation, each beam is further split into many pencil beams.) Through the iteration of the driven current profile calculations, each beam power is automatically controlled so that any deviation between the driven current profile and a preset objective current profile may be minimized. The objective profile has been chosen as $j = j_0(1 - s^2)^{0.5}$ throughout the present

T_e and n_e dependence calculations, where $s = r_\psi/a$ and r_ψ is the half width of flux surface labeled by ψ. Spatial profiles for T_e and n_e are also shown in Table 1. The T_e profile is parabolic and the n_e profile is very broad. The driven current profile for $\bar{n}_e = 0.7 \times 10^{20}$ m^{-3}, $\bar{T}_e = 20$ keV is found in Fig. 13-b.

The T_e dependence for γ is plotted in Fig. 4. The T_e dependence is weaker than linear. In the 10 keV $\leq \bar{T}_e \leq$ 30 keV range, γ is written by a following functional approximation;

$$\gamma = 0.064 (\bar{T}_e/\text{keV})^{0.58} \quad . \tag{15}$$

The n_e dependence of γ and the shinethrough fraction f_s are plotted in Fig. 5. In the regime $\bar{n}_e > 0.4 \times 10^{20}$ cm^{-3}, the shinethrough is small enough (less than 6 %), thus γ depends weakly on $\bar{n}_e$. In this range, the change in beam power deposition brings about a small γ-degradation with $\bar{n}_e$. On the other hand, the shinethrough fraction increases rapidly as $\bar{n}_e$ decreases below 0.4×10^{20} m^{-3}. Therefore, in this low density range, γ depends on $\bar{n}_e$ exponentially.

In the $0.1 \leq \bar{n}_e/10^{20}\text{m}^{-3} \leq 1.0$ range, γ is approximately given by

$$\gamma = 0.355\ \bar{n}_e^{-0.092} \{1 - \exp(-7.5\bar{n}_e)\} \tag{16}$$

with $\bar{n}_e$ in 10^{20} m^{-3}.

Although Eq. (16) is obtained with $\bar{T}_e = 20$ keV, it is expected that the beam power deposition characteristics may depend on $\bar{T}_e$ weakly. Therefore, the convenient functional

approximation of γ, including the n_e and T_e dependences, can be reduced from Eqs. (15) and (16);

$$\gamma \simeq 0.0624 \bar{T}_e^{0.58} \bar{n}_e^{-0.092} \{1 - \exp(-7.5 \frac{L}{L_0} \bar{n}_e)\} \qquad (17)$$

($\bar{T}_e$ in keV and $\bar{n}_e$ in 10^{20} m^{-3})

$$10 \leq \bar{T}_e/\text{keV} \leq 30, \quad 0.1 \leq \bar{n}_e/10^{20} m^{-3} \leq 1.0$$

$$L/L_0 = \sqrt{(R_0 + a)^2 - R_{tang}^2} \; / \; 4.28$$

The factor L/L_0 in Eq. (17), which is the ratio of beam paths, is added in order to give some generality to this formula for small change in the plasma size. This treatment will give a good approximation of γ for the reactor parameters close to INTOR parameters A in Table 1. The formula deviation from the numerical simulations is shown in Fig. 6, where the formula has been compared with the simulations in $10 \leq \bar{T}_e/\text{keV} \leq 30$, $0.1 \leq \bar{n}_e/10^{20} m^{-3} \leq 1.0$, $4.1 \leq R_0/m \leq 5.8$ ranges. The formula error is within +10 %, -2 % in these parameter ranges. Note that this formula is valid for the 500 keV beams only.

3.2 T_e dependence with a retained beta

The T_e dependence for current drive efficiency I_p/P_b is plotted in Fig. 7, where the beta value due to the thermal pressure is retained at 5.9 %. Thus, the density is not constant ($\bar{n}_e = 0.93 \times 10^{20}$ m^{-3} at $\bar{T}_e = 20$ keV). In this calculation, reactor parameters B (Table 2) are used.

The beam parameters are listed in Table 3. From Fig. 7, the T_e dependence of I_p/P_b for constant β is written by

$$\frac{I_p}{P_b} = 6.65 \times 10^{-4} \ (\overline{T}_e/\mathrm{keV})^{1.58} \quad . \tag{18}$$

This T_e dependence is consistent with the formula (17), because $\beta \propto \overline{n}_e \overline{T}_e$ is retained constant in the present calculation, whereby $\gamma \propto \overline{n}_e (I_p/P_b) \propto (I_p/P_b)/\overline{T}_e \propto \overline{T}_e^{0.58}$.

Increasing T_e with a constant beta usually results in a reduction in fusion power, while the drive efficiency I_p/P_b is increased. Therefore, a Q value (= fusion power/driver power) tends to saturate with $\overline{T}_e$ over 20 keV. The Q value is also shown in Fig. 7. The Q value is almost constant in the 25 keV $\leq \overline{T}_e \leq$ 30 keV range. In the over 30 keV range, Q reduces gradually.

Although the maximum Q value is obtained with $\overline{T}_e \gtrsim$ 30 keV, a net output power is usually maximized at $\overline{T}_e \gtrsim$ 20 keV, where 'net' means (total electric output) - (electric power for driver). Also, the maximum fusion output is generated with $\overline{T}_e \gtrsim$ 10 keV. Then, the operating temperature should be chosen in accordance with the experimental task. For a demonstration to commercial use, the optimum temperature should be about 20 keV.

Finally, it should be noted that the power balance between the injection power and the loss power from the plasma is not discussed in the present Q calculation. As shown in Ref. [18], including the power balance calculation

with a transport model may result in a lower Q value than that of the present calculation, owing to the operating parameter range restricted by the power balance condition.

3.3 Z_{eff} dependence and neo-classical effects

Current drive efficiencies I_p/P_b (Amp/Watts) and Q value (= fusion power/driver power) for INTOR are plotted in Fig. 8. Reactor parameters B used here are listed in Table 2. In Fig. 8, the solid line values are calculated with the finite aspect model of neo-classical trapped electron effect [8]. The broken line values are the case without trapped electrons. If the present neo-classical model is valid, the Z_{eff} dependences of I_p/P_b and Q value are very weak, in the $1.5 < Z_{eff} < 3.0$ range. On the other hand, without the trapped electron correction, the efficiency and Q value are greatly reduced, and high Z_{eff} operation will be required to obtain an acceptable drive efficiency.

In recent beam current drive experiments in JET and TFTR [11,12], the driven currents have shown a fairly good agreement with the values estimated by the neo-classical model. Therefore, the uncertainty over the existence of the trapped electron effects seems to be greatly reduced by these experiments. Throughout this paper, the full neo-classical effects [8] are used in the driven current calculations.

3.4 Beam energy dependence and Alfvèn wave instability

The current-drive efficiency strongly depends on the beam energy. The local current drive efficiency j/p_d, where j is the driven current density and p_d is the absorbed beam power density, is maximized when injection energy $E_b \approx 4\ E_c = 4\ (\frac{1}{2}m_b v_c^2)$ [v_c: see Eq. (3)]. For $\overline{T}_e \approx 20$ keV, this optimum injection energy is about $1.5 \sim 2$ MeV. When injection energy E_b exceeds this optimum, j/p_d gradually decreases, while it is rapidly reduced with $E_b < 2E_c$.

In order to discuss global current drive efficiency I_p/P_b, beam penetration and shinethrough must be taken into account. Considering deutrium beams, over several MeV injection is not desirable, because it usually results in a heavy shinethrough. Then, the energy from several hundred keV to 2 MeV is an acceptable range for the next generation tokamaks. (In this section, the MeV beams future development feasibility is not discussed. The use of heavy impurity beams is also out of the scope for this paper.)

As the fast ion velocity can exceed the Alfvèn velocity with the over several hundred keV injection, the Alfvèn waves may be generated and absorb the fast ion energy. The beam ions would be rapidly slowed to the Alfvèn velocity [9,13]. The Alfvèn wave effect existence is ambiguous, because no experiment has been reported to date with such high energy injection.

The E_b dependence of I_p/P_b and the drive efficiency degradation, due to Alfvèn wave instability (A.W.I.), is shown in Fig. 9, where parameters B (Table 2) are used. In order to take into account the A.W.I., in this calculation, it is assumed that the injected beam ions are immediately slowed down to the Alfvèn velocity, after being trapped in the plasma. The beam energy with the Alfvèn velocity, E_A, is about 500 keV when $\bar{T}_e$ = 20 keV, $\bar{n}_e = 0.93 \times 10^{20}$ m^{-3} and $\bar{n}_i = 0.87 \times 10^{-20}$ m^{-3} (Z_{eff} = 2.0). Therefore, the current drive efficiency for over 500 keV beams is greatly reduced by the A.W.I., while there is no degradation when E_b < 500 keV. As the over 500 keV beam is indispensable to drive currents with reasonable beam power in future large tokamaks, the A.W.I. investigation is a very critical issue.

Without the A.W.I., the optimum injection energy is about 1.5 MeV, as shown in Fig. 9.

The case with a lower density $\bar{n}_e = 0.7 \times 10^{20}$ m^{-3} is shown in Fig. 10, where Z_{eff} = 1.8. It was found that the optimum energy is reduced down to 1 MeV. This is because the shinethrough has increased for over 1 MeV beams.

3.5 Charge Exchange Loss Effect

The beam driven currents can be reduced by charge exchange loss of fast ions during the slowing down process. A detailed study report on the charge exchange loss effect is found in Ref. [3].

The efficiency reduction, due to the charge exchange

loss, is shown in Fig. 11, where parameters A in Table 1 are used. The neutral atom distribution in a plasma is assumed as

$$n_0(r) = 10^{\alpha_0 - 2 + 2s} \quad (m^{-3})$$

where $\alpha_0 = \log_{10}(n_{0\ edge})$ and $s = r_\psi/a$.

When $n_{0\ edge}/\bar{n}_e$ exceeds about 10^{-5}, the γ-deterioration becomes appreciable due to the charge exchange loss.

The current profile has been retained $(1 - s^2)^{0.5}$ profile, in this calculation. If the beam power distribution is retained, the current profile would become peaky, because of the charge exchange loss in the cold edge region.

3.6 Dependences on n_e and T_e profiles

The global current drive efficiency should depend on the plasma density profile and the temperature profile. In this paper, the following profiles are used to estimate the driven currents;

$$T_e = T_{eo}(1 - s^2)^{\alpha_T} \tag{19}$$

$$n_e = n_{eo}(1 - s^2)^{\alpha_n} \tag{20}$$

where $s = r_\psi/a$, again.

In the previous sections, values has been kept so that $\alpha_T = 1.0$ and $\alpha_n = 0.3$. The γ-dependence on α_n and α_T is shown in Fig. 12, as function of α_n, where A, B and C are the cases of $\alpha_T = 0.5$, 1.0 and 1.5, respectively, where parameters A in Table 1 are used. The fusion output depends

on the T_e and n_e profiles. Then the Q values are also plotted in Fig. 12. The broken line regime in the γ-plots means that it has been impossible to keep the required current profile [$\propto (1-s^2)^{0.5}$] in such regime ($\alpha_n \gtrsim 1.0$). It was found that peaked temperature profiles always reduce both γ and Q. On the other hand, the γ-dependence on α_n is not simple. One of the reasons for this complicated γ-dependence is that the power deposition characteristics are very sensitive to the density profile, while the sensitivity to the temperature profile is weak. Nevertheless, if one considers the Q value, instead of γ, Q increases monotonically with the density profile peaking. It will result in a broad temperature and a peaked density will give the largest Q value. Then, it implies a possibility of Q enhancement by the peaked density profile produced by pellet injections etc.

3.7 Characteristic change by R_{tang} variety

The γ-values and f_s are shown in Table 5 for various R_{tang}. It was found that an increase in R_{tang} results in a larger γ, while the shinethrough is enhanced. A similar result had been reported in Ref. [19]. In the case of $R_{tang} > R_0$, the current profile is intrinsically hollow. As shown in the following, the hollow profile slightly improves the γ-value. Note that the No. 7 and No. 8 beams are switched off for $R_{tang} > R_0$, in order to avoid direct shinethrough.

4. Current Density Profile Control

4.1 Current density profile tailoring

The current profile, driven by beam injection, depends on the beam line orientation. Using these characteristics, current profile tailoring is possible. A method proposed in Ref. [19] is based on the variation in R_{tang} values. In Ref. [18], the authors also proposed a current profile control method, where a rectangular shaped beam line cross-section with a large height is used and the beam power profile on vertical plane is controlled for tailoring the current profile. In the former method, the R_{tang} change will encounter difficulty due to the physical limitations caused by toroidal field coils spacing, especially when $R_{tang} > R_0$. The latter method may be limited by the maximum port size in height. In this study, the authors will analyse the latter method. The rectangular beam line will split in multi beam lines arranged in a vertical row. Each power is changed to take into account the power profile variety. This method is same to used in Ref. [20]. The current profile control by the vertically arranged multi beams was later proposed independently by the authors of Ref. [16].

4.2 Current density profile control ability

Throughout the calculations by the beam current drive analysis code, the injected beam line (with rectangular cross-section H x W) is split into multi beams. In the present study, the beam line is split into 16 beams, as shown in Table 3. Each beam has a cross-section of 0.4 m in width and

0.2 m in height. Individual beam centerlines are parallel ($\theta_v = 0$, see Fig. 3) to the horizontal plane, but are vertically shifted with Z_h from the tokamak equatorial plane. Assuming symmetrical injection in respect with the equatorial plane, the beam deposition is calculated in the upper half plasma with 8 beams. Each vertically shifted beam drives the current in a toroidal shell with a minor radius in accordance with Z_h. Therefore, driven current tailoring is possible by control of individual beam powers.

The beam current drive analysis code, used in this study, has a routine to automatically control each beam power in order to obtain a required current profile. Through the iterative current profile calculations, the beam powers, to minimize the deviation between the driven current profile and the preset objective (required) profile, are determined.

Driven current profiles on the equatorial plane for various objective profiles are shown in Fig. 13 with the beam power distribution on the vertical plane. Flux surfaces for parameters A are shown in Fig. 14. (The actual r_ψ mesh number is 100, while 10 flux surfaces are plotted.) It was found that the current profile control ability is very flexible. Parabolic and very flat profiles have been generated as well as the hollow profile. The deviation between the driven profile and the objective profile is less than 2 %, except for the central small bumps and the edge region ($r_\psi/a > 0.85$). Since the central bumps are removable with a finer control of the central beams ($Z_h < 0.5$ m),

they are not essential imperfection.

The γ-value is almost independent from the current profiles. As the current profile flattens and hollows, the beam powers injected near the plasma edge increases gradually. This results in more shinethrough, as shown in the figure. In the hollow 2 profile (Fig. 13-e), most of the power is injected in regime Z_h > 1.0 m, and shinethrough fraction f_s, averaged in the total power, is about twice as large as for the parabolic case. The average shinethrough seems to still be small (∿ 1.5 %), but most of shinethrough occurs in beams No. 7 and 8. Generally speaking, when Z_h exceeds 0.7 κa, the shinethrough fraction rapidly increases. In the present case, beam shinethrough values for No. 7 or No. 8 are over 5 %, while beam shinethrough values for Nos. 1 ∿ 6 are comparably small (≪ 1 %).

Although the 3.2 m total beam line height exceeds 85 % of plasma height, the current profile control ability seems to be still insufficient near the plasma edge to drive the flat or hollow current profile. Increasing the beam height may be very difficult because of the physical limitation in regard to the injection port size imposed by the size and spacing of toroidal coils and blanket. Moreover, beam injection with a larger Z_h will result in a still heavier shinethrough. The shinethrough limit and the injection port size are essential limitation for the current profile control ability of beam current driver.

If an additional 9th beam with Z_h = ±1.7 is permissible (total beam height H is, now, 96 % of plasma height!), the

edge profile control ability is much improved, as shown in Fig. 15, where the objective profile is 'Hollow 2' in Fig. 13. The profile deviation is less than 2 % in the whole region except for the central bumps. The averaged shinethrough has been increased up to 6.7 %. Most of power loss occurs in the No. 9 beam.

As beam height H decreases, the current profile control ability is reduced, especially in the plasma edge. The driven current profiles with various H are compared in Fig. 16. When vertical angle $\theta_v = 0$, the large Z_h beams are indispensable to drive a broad profile current.

Use of non zero θ_v beams allows controlling the edge current profile, even when the beam height is restricted to within a moderate value. The current profile in Fig.17 is driven by 4 beam lines. The first beam line is injected with $\theta_v = 0$, beam height H = 2.4 m (65 % of plasma height). This is identical to the beams Nos. $1 \sim 6$ in Table 3. Other 3 beam lines are set at $\theta_v \neq 0$ as listed in Table 4, while the injection positions Z_h are kept at 1.1 m. These angle beams increase the profile control ability, but also reduce drive efficiency γ, and the shinethrough is still an essential limitation.

5. Transformer Recharging

5.1 Plasma and beam parameters

Transformer recharge operation is possible with the same beam system as that used in heating and burning phases.

The authors used the same beam parameters in Table 3 except that beams No. 7 and 8 are switched off in order to reduce the shinethrough. Beam energy is 500 keV. This is higher than the benchmark value, E_b = 400 keV, decided upon in the INTOR workshop [14]. The plasma density range is $0.8 \leq \bar{n}_e/10^{19}\ m^{-3} \leq 1.4$. This value is also higher than the benchmark value, $\bar{n}_e = 0.6 \times 10^{-19}\ m^{-3}$. First of all, the reasons for the parameter choice will be given.

The low beam energy, to reduce shinethrough, is not advisable, because the shinethrough reduction is cancelled by the beam power increment owing to the current drive efficiency deterioration. In Fig. 18, beam power P_b to drive 10 MA and shinethrough power $f_s \cdot P_b$ are plotted as functions of beam energy E_b, where reactor parameters A is used with $\bar{n}_e = 10^{19}\ m^{-3}$, $\bar{T}_e = \bar{T}_i = 10$ keV. The solid lines are the case with the beam line height H = 2.4 m, i.e. No. 7 and 8 beams are switched off. With increasing E_b, f_s increases but P_b decreases. In a result, $f_s \cdot P_b$ is almost constant for $0.2\ MeV \leq E_b \leq 1.0\ MeV$. When the beam power density is retained, the wall heat load due to the beam shinethrough is proportional to $f_s \cdot P_b$. Therefore, there is no merit in lowering E_b. Moreover, the wall particle load is increased by lowering E_b. On the other hand, the authors' time dependent quasi-1D

transport analysis [15] has shown that a first difficulty for the transformer recharge operation with NBI is to exhaust the injected beam particles, in order to keep a very low density. To reduce the number of beam particles, a higher beam energy is advisable. The 1 MeV beam would be the best, if possible. However, in the beam technology limitation point of view, the 500 keV beam system, used in the burning phase, is a reasonable choice.

Throughout this section, the f_s values are somewhat larger than the values in Ref. [16]. The reason is that beam height H used in the present study is still very large (2.4 m) while beams No. 7 and 8 have been switched off. This beam can drive acceptable parabolic profile currents. An example of the driven current profile is shown in Fig. 19. If beams No. 3∿6 are also switched off (H = 0.8 m), f_s is reduced by 3/4. The broken lines in Fig. 18 are shown P_b and $f_s \cdot P_b$ for H = 0.8 m. However, the driven current profile by such a beam is quite peaky, as previously shown in Fig. 16, wherely it would result in q(0) less than unity and MHD instabilities.

When assuming 500 keV beam, the number of particles input rate for P_{abs} = 50 MW attains 3×10^{18} $m^{-3}sec^{-1}$. Since the particle exhaust time constant in the INTOR size tokamak will be several seconds, keeping a low density below 10^{-19} m^{-3} would be difficult. The quasi-1D transport analysis [15] has shown that maintaining a density below 10^{19} m^{-3} is very difficult with any confinement scalings proposed to date. Therefore, the authors have chosen comparably

high densities in this study ($0.8 \leq \overline{n_e}/10^{19}$ m$^{-3} \leq 1.4$).

5.2 Results from parameter scan

During the transformer recharging, the ion and electron temperatures should satisfy the steady state power balance. In order to determine these temperatures, the authors have combined the beam current drive analysis code with O-D power balance code, which is based on a 2 flow transport model and includes various impurity radiation data. A neo-classical ion confinement time is assumed. An electron energy confinement time is almost identical to a global energy confinement time τ_E. Various τ_E scalings have been proposed to date, but no scaling is fairly reliable for the transformer recharging parameters (extreme power in very low density with hgih Z_{eff}). Therefore, in this study, the authors have used a most basic scaling, INTOR/ALCATOR type,

$$\tau_E = 0.69\overline{n_e}(10^{20}\ \text{m}^{-3})\{a(\text{m})\}^2\kappa \quad . \tag{21}$$

The τ_E values for $\overline{n_e}/10^{19}$ m^{-3} = 0.8, 1.0, 1.2 and 1.4 are 0.12, 0.15, 0.18 and 0.21 sec, respectively. Note that the Goldston L-mode scaling [17] gives a <u>better</u> confinement under the present extreme plasma condition, i.e. $\tau_E(G-L) = 0.3$ sec with I_p = 8 MA and P_{abs} = 50 MW. The INTOR/ALCATOR scaling gives a lowest τ_E value in various scalings for such a low density regime.

In the driven current analysis, the electron density and the absorbed beam power P_{abs} are given first. Then

the ion and electron temperatures are determined by power balance code. Throughout this study, 1 % X_e impurity is assumed. The Z_{eff} value depends on the temperature, because the X_e ion charge state changes with changing T_e. The impurity radiation rate also changes with changing T_e. The beam current drive analysis code estimates shinethrough f_s, driven current I_D and P_b [= $P_{abs}/(1 - f_s)$], using $\bar{T}_e$ and Z_{eff} obtained by power balance code. Return OH current I_{OH} is determined by

$$I_{OH} = 2\pi R_0 E/R_p \tag{22}$$

where E = -0.01 (V/m) and

$$R_p = 1.0 \times 10^{-7} \ (Z_{eff}/1.5) \left(\frac{2}{\bar{T}_e}\right)^{1.5} \quad (\Omega) \quad . \tag{23}$$

The parameter scan result is shown in Fig. 20 and some data are listed in Table 6. From Fig. 20, the beam power, to sustain $I_D + I_{OH}$ = 8 MA, can be determined. The 47 MW to 60 MW power is required for $0.8 \leq \bar{n}_e/10^{19}\ m^{-3} \leq 1.4$. As the current drive power in the burning phase is 74 MW for reactor parameter A, the same beam system can be used for transformer recharging. The shinethrough can be reduced by raising the density, while the beam power increases.

The operational parameters in the transformer recharge phase are summarized in Table 7. The γ-value increases with n_e, but I/P is retained almost constant.

6. Fast Beam Ions Pressure

Pressure generated by the circulating beam ions (so called 'beam pressure') is not a negligible value in contrast with most other r.f. current drive methods where the current carrying electron pressure is usually small.

The β-values are plotted in Figs. 21 and 22 as functions of $\bar{T}_e$ and $\bar{n}_e$, respectively, where reactor parameters A is used. (The γ-values with these parameters have been shown in Figs. 4 and 5, previously.) Beta value due to the fast alpha pressure, β_α, increases with n_e and T_e as well as the beta value due to the thermal pressure, β_{th}. On the other hand, the beta value due to beam pressure, β_b, is retained almost constant. As the beam beta is proportional to the driven current I_D, the following formula for β_b is obtained for INTOR size tokamak;

$$\beta_b = 1.2\ \% \left(\frac{5.5T}{B_t}\right)^2 \left(\frac{I_D}{8MA}\right) \left(\frac{2.2m}{a^2\kappa}\right) . \qquad (24)$$

This formula is approximately applicable to the transformer recharge phase, where the thermal beta (∿ 0.3 %) is negligible in comparison with the beam beta (∿ 2 %).

If the beam beta should be taken into account in a beta limit scaling, like the Troyon's scaling, the beam pressure existence may be a critical drawback for the beam current drive. On the other hand, the higher total pressure in the transformer recharge phase (∿ 30 % of burning phase pressure), would reduce cyclic stress on poloidal coils [18]. Therefore, the beam pressure can be an advantage of

the beam current driver for transformer recharging.

If a full non-inductive current ramp-up is required in the initial phase of operational scenario, special attention should be paid to the existence of finite beam pressure. The beam pressure immediately attains its steady state value within the beam-ion slowing down time t_b, but the current ramp-up time depends on the plasma skin time L_p/R_p, which is usually much longer than t_b. As a result, the beam pressure could exceed the poloidal and the toroidal beta limits during the initial current ramp-up phase, where $t_b < t < L_p/R_p$ [15].

7. Conclusion

Benchmark parameters in Table 1 and Table 3 give $I/P \gtrsim 0.108$ (A/W) and $\gamma \gtrsim 0.37$. Then, 74 MW injection will drive 8 MA current. The γ-scaling formula, on the reactor size and the plasma parameters, is derived [formula (17)].

The current density profile control ability is very flexible. Parabolic profile current can be driven, as well as flat and hollow profile currents, by the beam power profile control in the vertical plane. The γ-value is nearly independent from the current profile. The essential limitation, for profile control ability with NBI, is the shinethrough from the edge plasma region, while the port size restriction could be overcome if injection with some vertical angle were used.

The same beam system as the burning phase current driver is applicable for transformer recharging. Required beam power, to keep 8 MA current with a reverse electric field $E = -0.01$ V/m, is 50 to 60 MW. High density recharging with $\bar{n}_e$ over 10^{19} m^{-3} is possible and desirable. The shinethrough fraction can be moderate ($\sim$ 15 %) with $\bar{n}_e = 1.4 \times 10^{19}$ m^{-3}.

Although the negative ion beam technology development is a key issue for the beam driver, the current drive efficiency for the 500 keV beam is acceptable for the next generation tokamaks. If over 1 MeV beam is available, the beam current driver characteristics will be much improved.

Acknowledgements

The authors acknowledge Drs. S. Tamura, M. Yoshikawa, K. Tomabechi, S. Mori (JAERI), K. Shinya and H. Yamato (TOSHIBA Corporation) for their suport throughout this work.

References

[1] OHKAWA, T., Nucl. Fusion 10 (1970) 185.

[2] GAFEEY, J. D., J. Plasma Physics 16 (1976) 149.

[3] OKANO, K., Plasma Phys. and Control. Fusion 29(1987)1115.

[4] D. R. SWEETMAN, Nucl. Fusion, 13 (1973) 157.

[5] OKANO, K., INOUE, N., UCHIDA, T., Plasma Phys. and Control. Fusion 27 (1985) 1069.

[6] OLSON, R. E., BERKNER, K. H., GRAHAM, W. G., PYLE, R. V., SCHLACHTER, A. S., STEARNS, J. W., Phys. Rev. Lett. 41 (1978) 163.

[7] SCHLACHTER, A. S., BERKNER, K. H., GRAHAM, W. G., PYLE, R. V., STERRNS, J. W., TANIS, J. A., Phys. Rev. A 24 (1981) 1110.

[8] START, D. F. H. and CORDEY, J. G., Phys. Fluids 23 (1980) 1477.

[9] MIKKELSEN, D. R. and SINGER, C. E., Nucl. Technol./ Fusion 4 (1983) 237.

[10] OHARA, Y. et al., Tokamak Concept Innovations, IAEA Technical Document, IAEA-TECDOC-373, P305, IAEA, Vienna (1986).

Acknowledgements

The authors acknowledge Drs. S. Tamura, M. Yoshikawa, K. Tomabechi, S. Mori (JAERI), K. Shinya and H. Yamato (TOSHIBA Corporation) for their suport throughout this work.

References

[1] OHKAWA, T., Nucl. Fusion 10 (1970) 185.

[2] GAFEEY, J. D., J. Plasma Physics 16 (1976) 149.

[3] OKANO, K., Plasma Phys. and Control. Fusion 29 (1987) 1115.

[4] D. R. SWEETMAN, Nucl. Fusion, 13 (1973) 157.

[5] OKANO, K., INOUE, N., UCHIDA, T., Plasma Phys. and Control. Fusion 27 (1985) 1069.

[6] OLSON, R. E., BERKNER, K. H., GRAHAM, W. G., PYLE, R. V., SCHLACHTER, A. S., STEARNS, J. W., Phys. Rev. Lett. 41 (1978) 163.

[7] SCHLACHTER, A. S., BERKNER, K. H., GRAHAM, W. G., PYLE, R. V., STERRNS, J. W., TANIS, J. A., Phys. Rev. A 24 (1981) 1110.

[8] START, D. F. H. and CORDEY, J. G., Phys. Fluids 23 (1980) 1477.

[9] MIKKELSEN, D. R. and SINGER, C. E., Nucl. Technol./ Fusion 4 (1983) 237.

[10] OHARA, Y. et al., Tokamak Concept Innovations, IAEA Technical Document, IAEA-TECDOC-373, P305, IAEA, Vienna (1986).

[11] CORDEY, J. G., 'Beam Current Drive in JET', in INTOR related specialists' meeting on non-inductive current drive, Sept. 15-17, 1986, Garching.

[12] GRISHAM, L. 'Currents Driven during beam heating on TFTR', Ibid.

[13] BERK, H. L. et al., Nucl. Fusion 15 (1975) 819.

[14] INTOR Phase two A, Part III, Session XIV, IAEA, Vienna (1987), to be published.

[15] MASUZAWA, M. et al., 'Plasma Current Ramp-up by Natural Beam Injector', to be published.

[16] EHST, D. A., EVANS Jr., K., MIKKELSEN, D. R., IGNAT, D. W. and MAU, T. K., Argonne National Laboratory Report, ANL/FPP/TM-213.

[17] GOLDSTON, R., Plasma Phys. and Control. Fusion 26 (1984) 87.

[18] YAMAMOTO, S. et al., in the 11th IAEA Int. Conf. on Plasma Physics and Controlled Fusion Research, Kyoto, 1986, IAEA-CN-47/H-I-3.

[19] OKANO, K. et al., Tokamak Concept Innovations, IAEA Technical Document, IAEA-TECDOC-373, P. 209, IAEA, Vienna (1986).

[20] OKANO, K. et al., 'Comparison of NBI Current Drive Theory with Experiment and Requirements for Extraporation to Next Step Devices', INTOR related specialists' meeting on Non-inductive Current Drive, Sept. 15-17, 1986, Garching.

Table 1 Reactor Parameters A

INTOR benchmark test parameters [14]

$R = 4.9$ m,	$a = 1.167$ m,	$R/a = 4.2$
$\kappa = 1.6$,	$d = 0.5$,	$B_t = 5.5$ T

$\bar{n}_e = 0.7 \times 10^{20}$ m^{-3}	$n_e \propto (1 - s^2)^{0.3}$
$\bar{T}_e = 20$ keV	$T_e \propto (1 - s^2)^{1.0}$ [$s = r/a$]
$I_p = 8$ MA	$j \rightarrow j_0(1 - s^2)^{0.5}$ (as close as possible)

$Z_{eff} = 2.0$ (X_e 0.04 %, He 5 %)

Table 2. Reactor Parameters B

Previous INTOR benchmark test parameters [20].

$R = 5$ m,	$a = 1.2$ m,	$R/a = 4.16$
$\kappa = 1.6$,	$d = 0.2$,	$B_t = 4.96$T

$\bar{n}_e = 0.93 \times 10^{20}$ m^{-3}	$n_e \propto (1 - s^2)^{0.3}$
$\bar{T}_e = 20$ keV	$T_e \propto (1 - s^2)^{1.0}$
$I_p = 6.4$ MA	$j \rightarrow j_0(1 - s^2)^{0.5}$ (as close as possible)

$Z_{eff} = 2.0$ (X_e 0.04 %, He 5 %)

Table 3 Beam Parameters

E_b = 500 keV, D^0 beam (W/O D_2^0, D_3^0)

Beam line cross-section shape

Rectangular 3.2 m x 0.4 m (h x w).

Minimum major radius of beam line axis

$$R_{tang} = \begin{cases} 4.3 \text{ m} & \text{(for parameters A)} \\ 4.7 \text{ m} & \text{(for parameters B)} \end{cases}$$

Vertical injection angle

$\theta_V = 0°$

Vertical beam axis shift from the mid-plane

$Z_h = 0$ m

(This beam line is split into 16 beams in the numerical code.)

Beam No.	Z_h/m	h/m	w/m	θ_v
1	±0.1	0.2	0.4	0
2	±0.3	0.2	0.4	0
3	±0.5	0.2	0.4	0
4	±0.7	0.2	0.4	0
5	±0.9	0.2	0.4	0
6	±1.1	0.2	0.4	0
7	±1.3	0.2	0.4	0
8	±1.5	0.2	0.4	0

Table 4 Vertical angle beams

Beam No.	Z_h/m	h/m	w/m	θ_v
7	±1.1	0.2	0.4	± 5°
8	±1.1	0.2	0.4	±10°
9	±1.1	0.2	0.4	±15°

Table 5. R_{tang} scan.

R_{tang} (m)	γ	f_s (%)	Comments
$R_0 - \frac{3}{4}a$: 4.0	0.351	0.68	Beam in Table 3
$R_0 - \frac{1}{2}a$: 4.3	0.369	0.92	↑
$R_0 - \frac{1}{4}a$: 4.6	0.376	4.2	↑
R_0 : 4.9	0.375	6.4	↑
$R_0 + \frac{1}{4}a$: 5.2	0.391	5.7	No. 7 & 8 beam s/w off Hollow profile
$R_0 + \frac{1}{2}a$: 5.5	0.387	8.1	↑

Table 6 Parameter scan for transformer recharging

(Reactor Parameters A)

$\overline{n_e}$ $10^{19}m^{-3}$	$\overline{T_e}$ keV	$\overline{T_i}$ keV	Z_{eff} (X_e 1%)	P_{abs} MW	P_b MW	f_s %	I_D MA	$-I_{OH}$ MA
1.4	5.2	5.4	13.5	30.0	35.4	15.3	4.6	1.4
1.2	6.2	6.5	13.6	30.0	37.4	19.8	6.0	1.9
1.0	7.1	7.7	13.7	30.0	40.5	25.9	7.8	2.3
0.8	7.9	9.3	13.8	30.0	45.4	33.9	10.4	2.6
1.4	8.2	8.8	13.9	40.0	47.4	15.6	8.0	2.8
1.2	11.6	13.5	15.0	40.0	49.7	19.5	10.5	4.3
1.0	11.6	14.2	15.0	40.0	53.5	25.3	12.7	4.3
0.8	11.6	16.3	15.0	40.0	59.9	33.2	16.0	4.3
1.4	12.7	14.2	15.6	50.0	58.8	15.0	11.5	4.7
1.2	13.8	16.3	15.9	50.0	61.9	19.2	13.8	5.3
1.0	13.9	17.7	16.1	50.0	66.6	24.9	16.6	5.3
0.8	14.5	23.3	16.1	50.0	74.0	32.4	20.9	5.6

Table 7. Recharging parameters summary.

(Reactor Parameters A)

$\overline{n_e}$ $10^{19}m^{-3}$	$\overline{T_e}$ keV	$\overline{T_i}$ keV	P_b MW	f_s %	γ	I/P A/W	I_D MA	$-I_{OH}$ MA
0.8	8.0	9.5	46.5	33	0.093	0.24	11.0	3.0
1.0	11.2	14.0	53.0	25	0.12	0.24	12.5	4.5
1.2	13.6	16.0	59.5	20	0.13	0.23	13.4	5.4
1.4	12.2	13.0	57.0	15	0.15	0.22	12.4	4.4

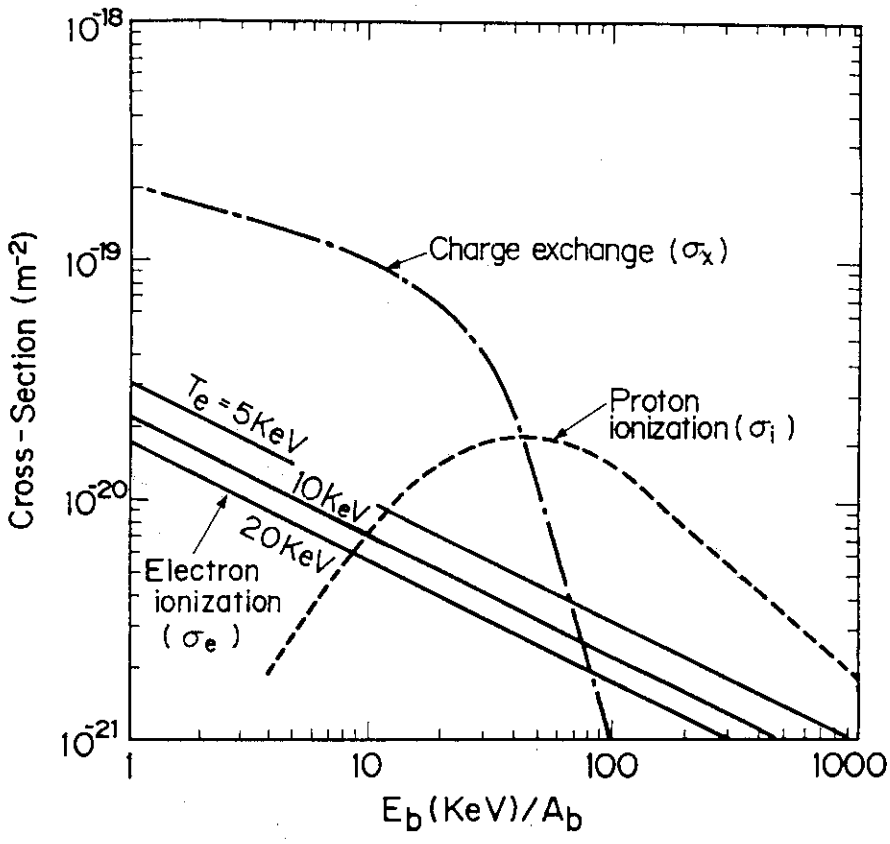

Fig. 1 Beam ionization cross-sections

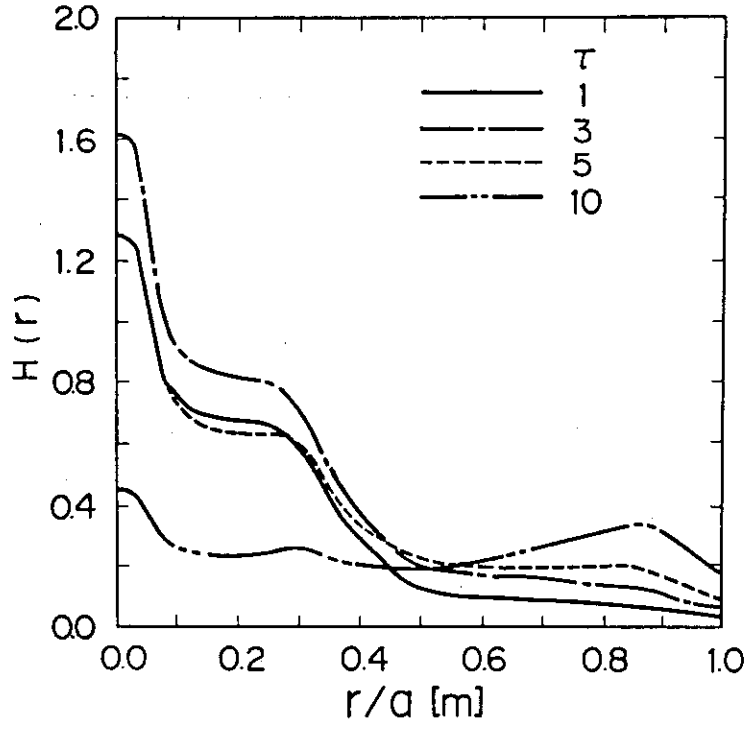

Fig. 2 Power deposition profiles for various τ, where τ is a beam pass integral of $n_e\sigma_{eff}$

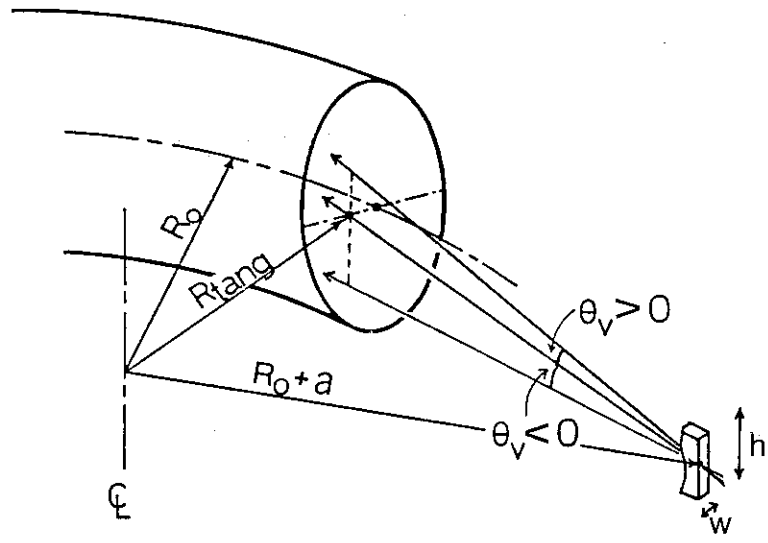

Fig. 3 Example of beam line orientations, for 3-D beam power deposition code. This figure is illustrated assuming that the vertical shift Z_h for beam axis is zero

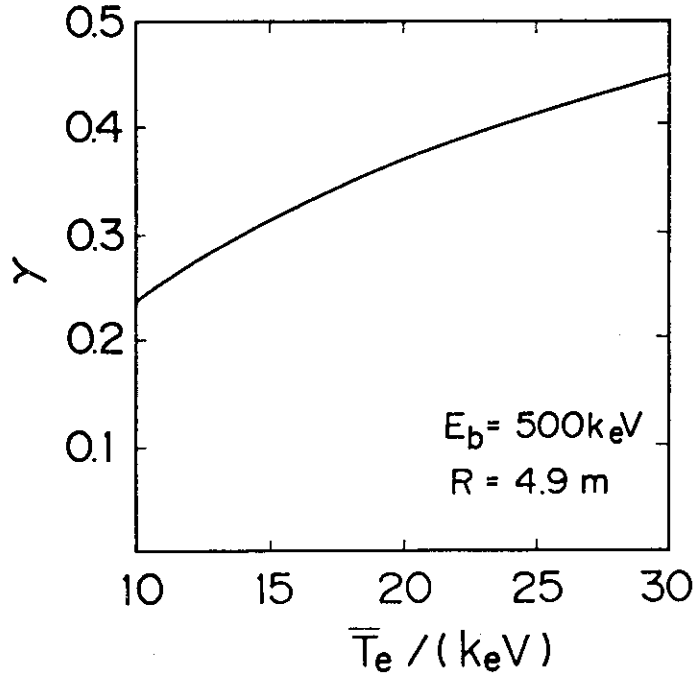

Fig. 4 T_e-dependence of γ
(Reactor Parameters A)

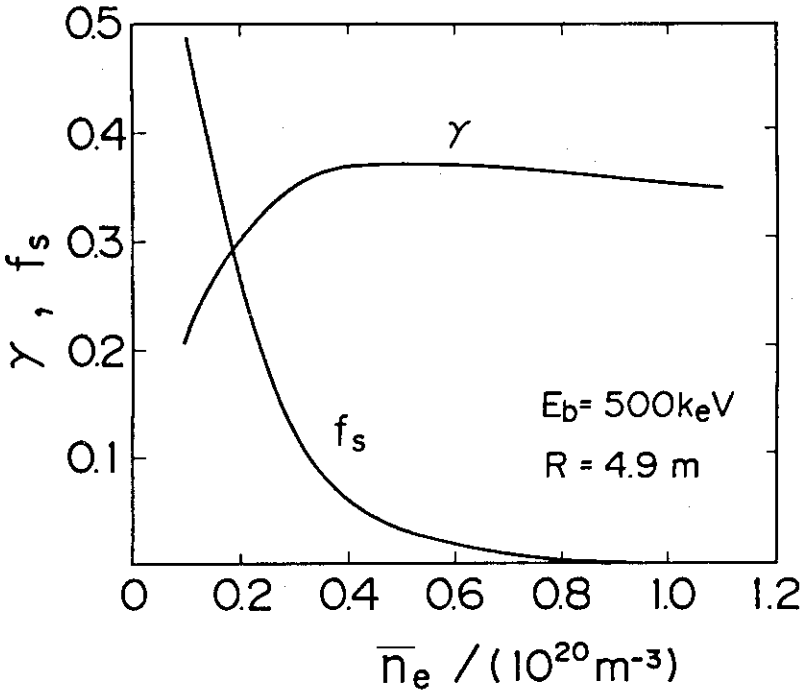

Fig. 5 n_e-dependence of γ and the shinethrough f_s (Reactor Parameters A)

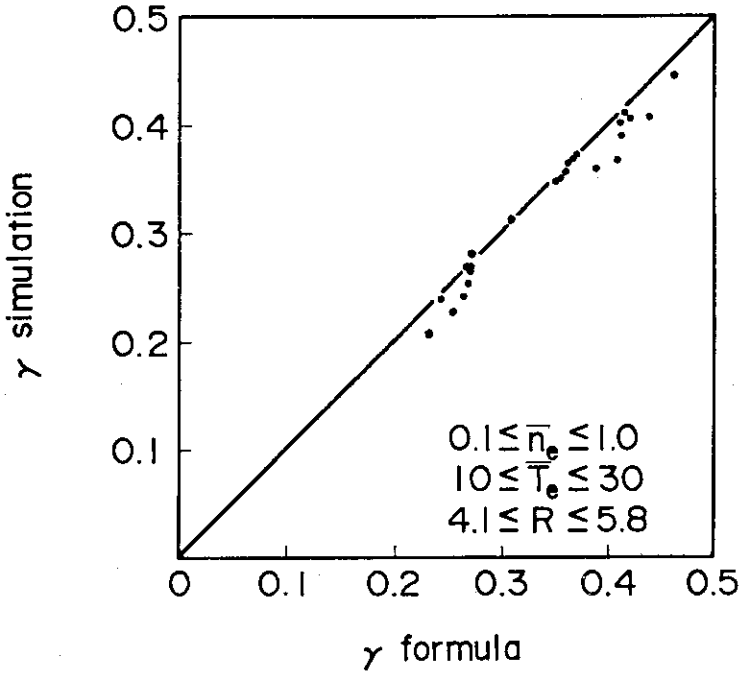

Fig. 6 Comparison between γ-formula and numerical simulation,
where $0.1 \leq n_e/10^{20}\ m^{-3} \leq 1.0$, $1.0 \leq T_e/keV \leq 30.0$ and $4.1 \leq R_0/m \leq 5.8$

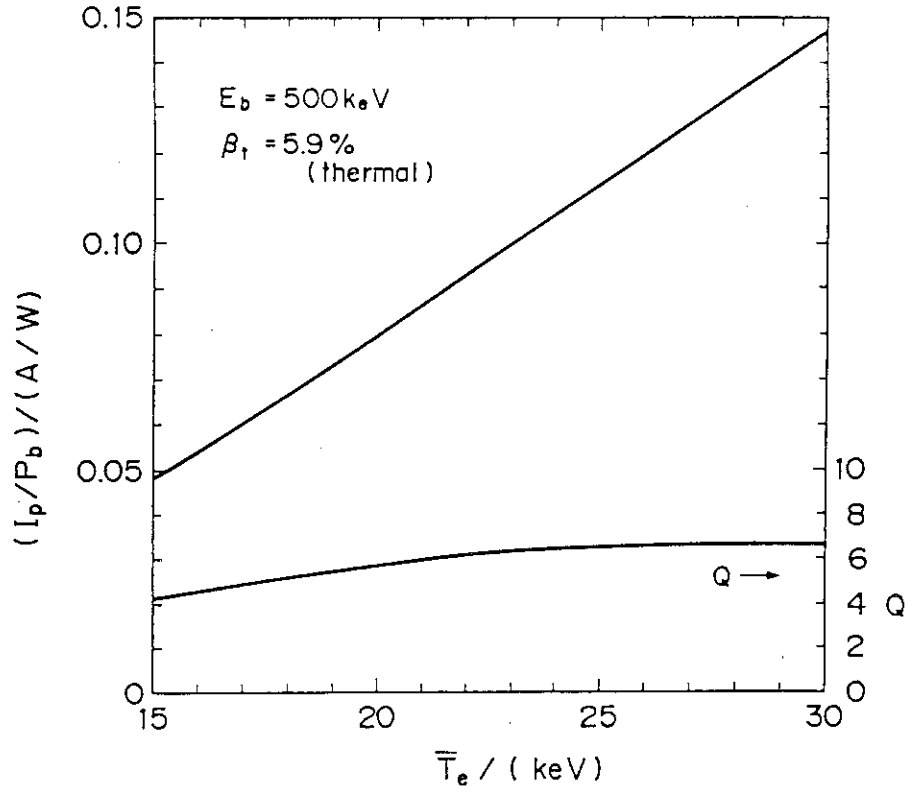

Fig. 7 T_e-dependence of I_p/P_b with retaining β_t = 5.9 % (Reactor Parameters B, [20])

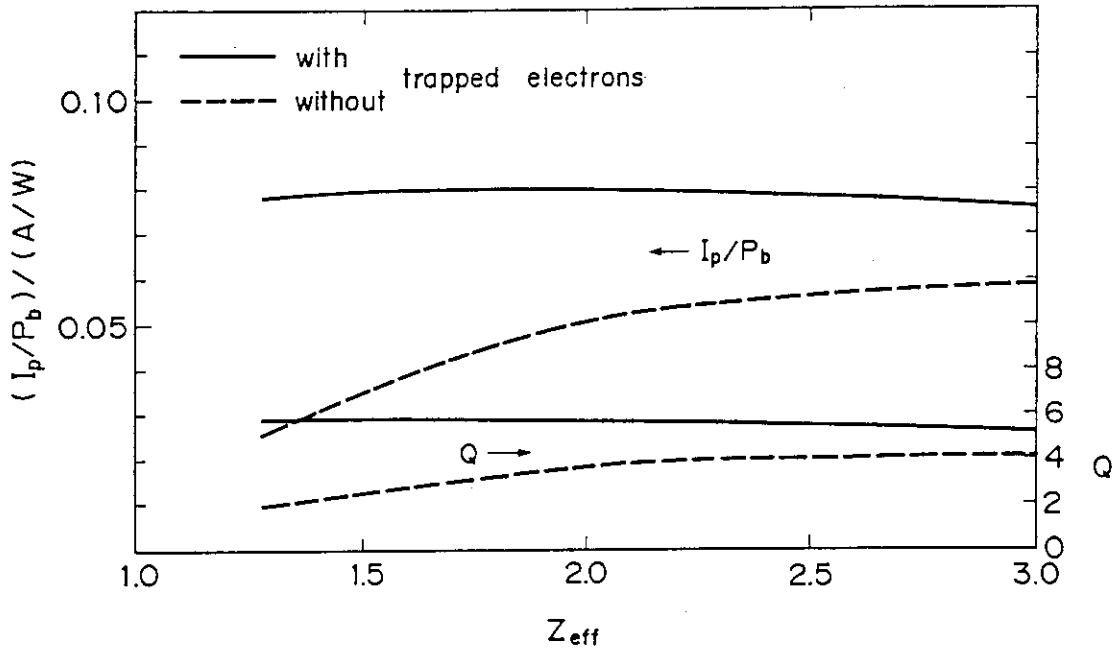

Fig. 8 Z_{eff}-dependences of I_p/P_b and Q value, with and without the trapped electron effects (Reactor Parameters B, [20])

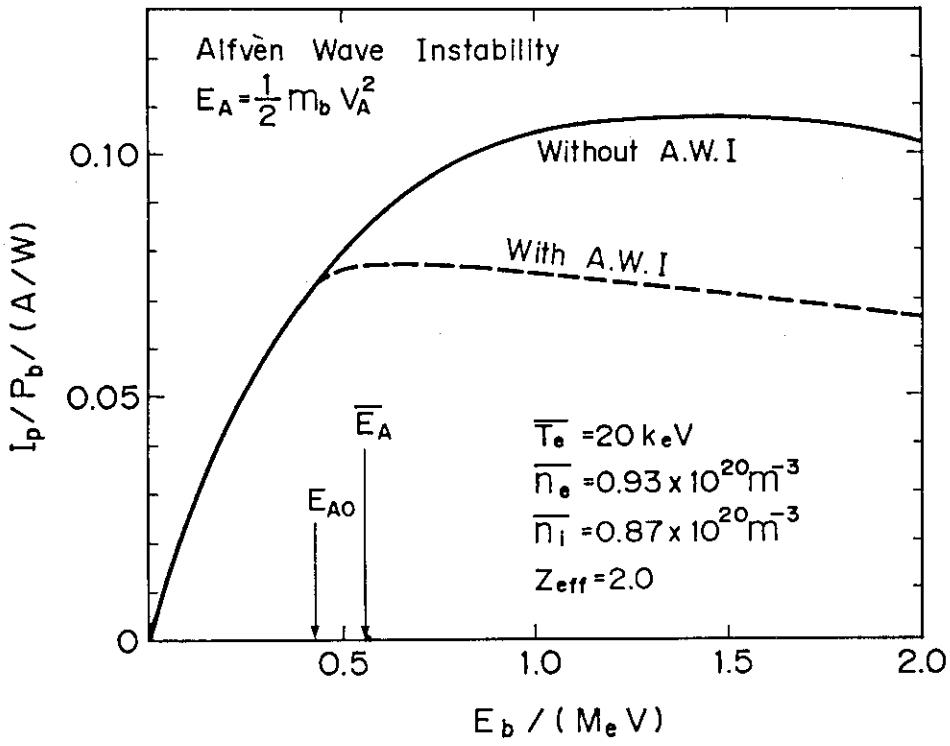

Fig. 9 Beam energy dependence of I_p/P_b, with and without the Alfvèn wave instability
(Reactor Parameters B, [20])

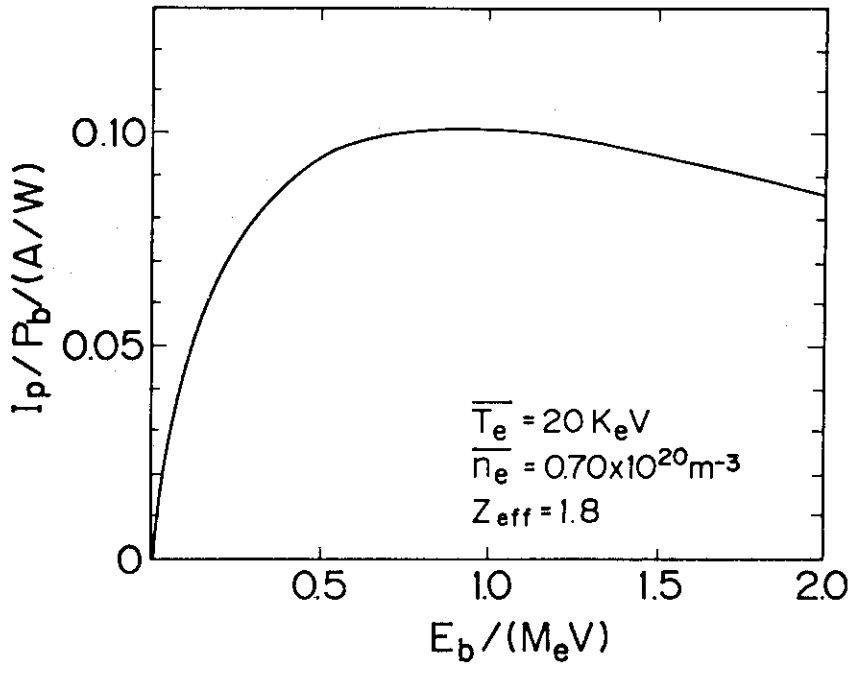

Fig. 10 Beam energy dependence of I_p/P_b
(Reactor Parameters B, but $\overline{n}_e = 0.7 \times 10^{20}$ m^{-3})

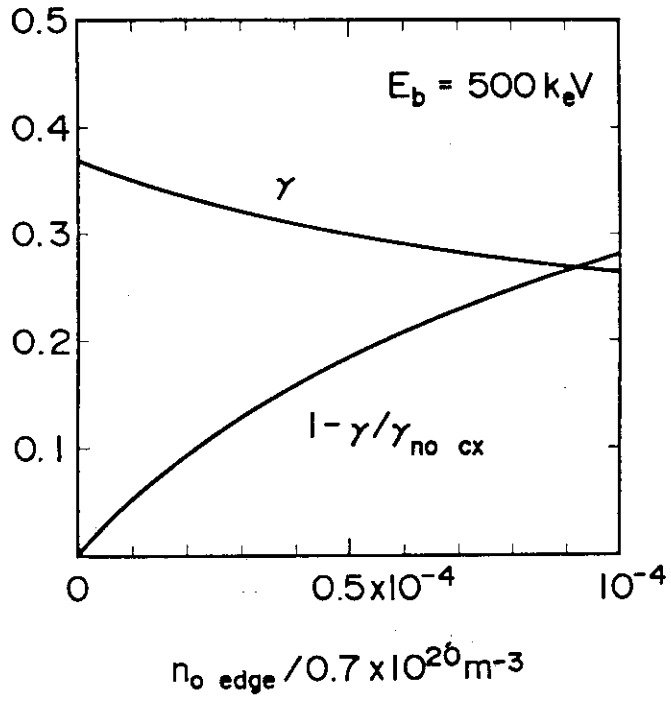

Fig. 11 Charge exchange loss effect on beam driven currents

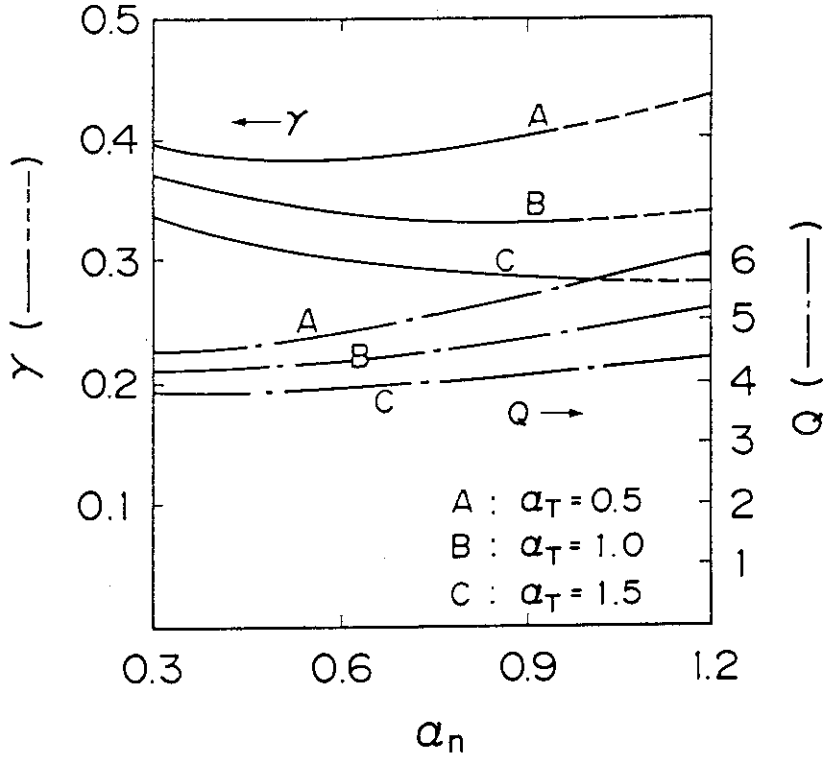

Fig. 12 γ-value dependence on the n_e and T_e profiles. $n_e = n_{eo}(1-s^2)^{\alpha_n}$, $T_e = T_{eo}(1-s^2)^{\alpha_T}$ (Reactor Parameters A)

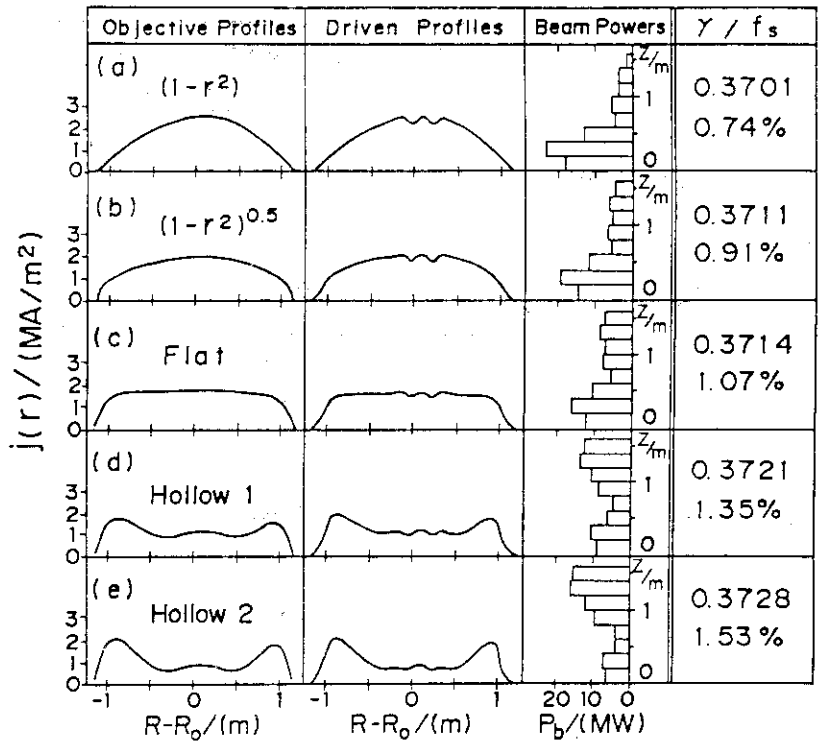

Fig. 13 Driven current profiles for various objective profiles, and required beam power distributions in vertical plane
(Reactor Parameters A)

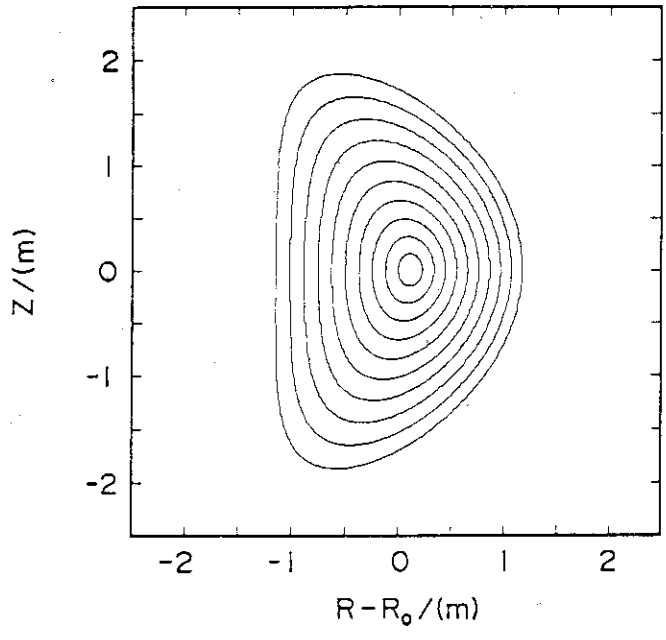

Fig. 14 Magnetic flux surfaces used in calculation with reactor parameters A. The actual mesh number is 100, while only 10 flux surfaces are shown

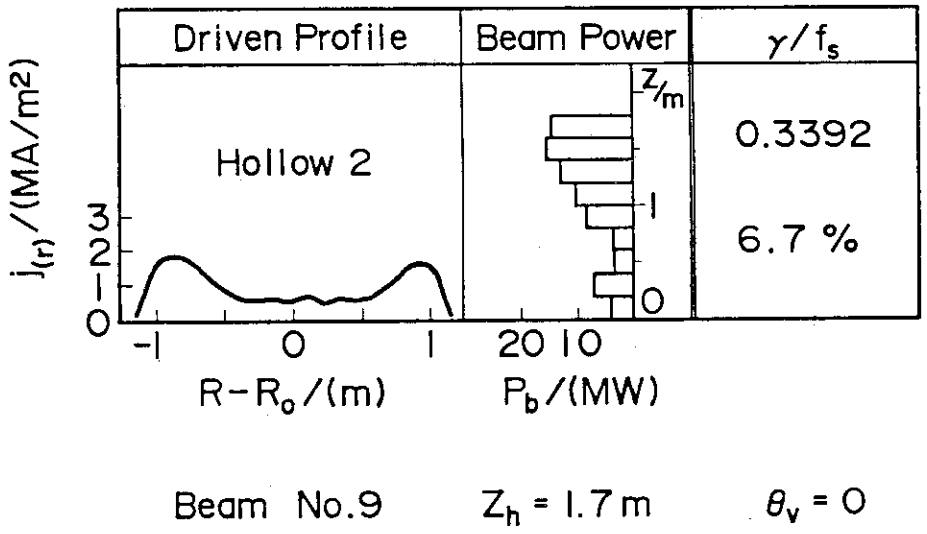

Fig. 15 Enhancement in current profile control ability by an additional No. 9 beam.
Compare with Fig. 13-(e)
(Reactor Parameters A)

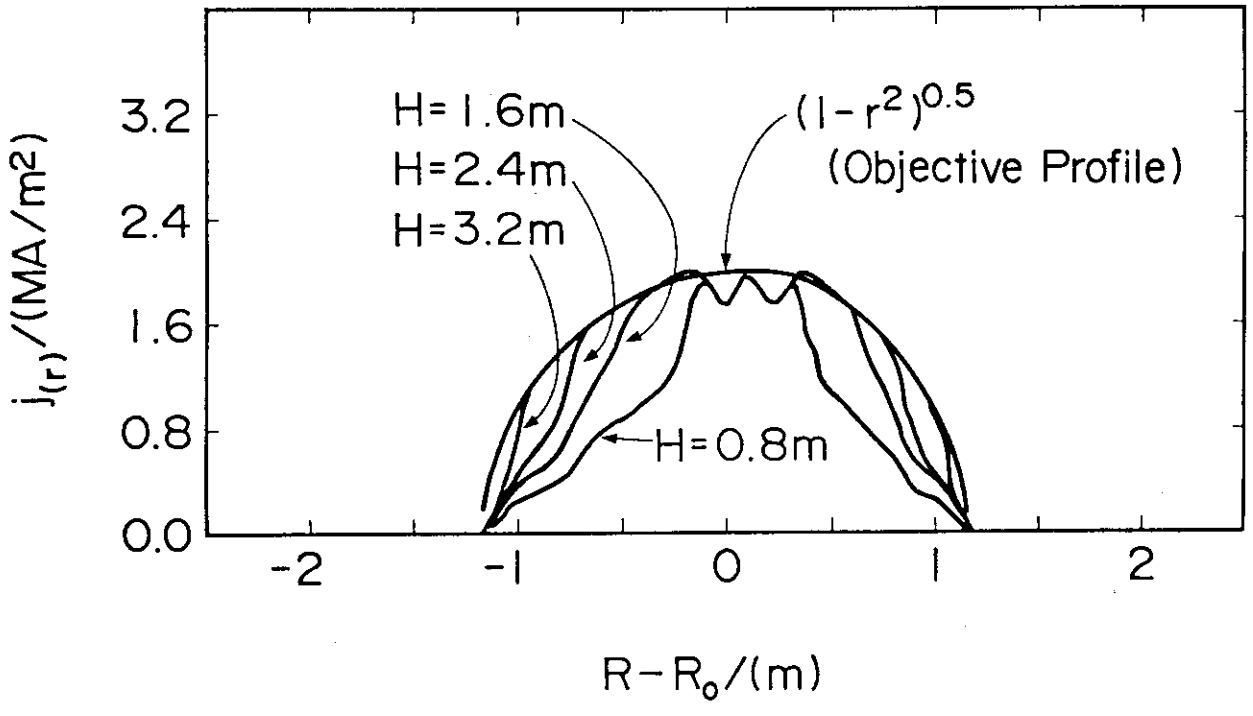

Fig. 16 Degradation in current profile control ability with decrease in beam line height H
(Reactor Parameters A)

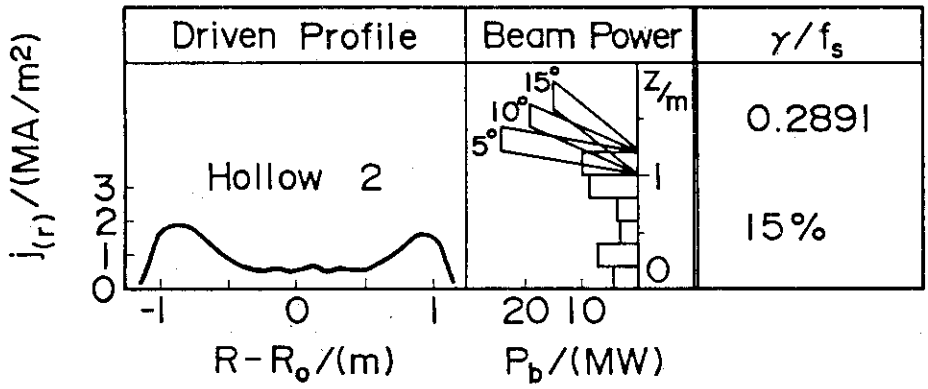

Fig. 17 Enhancement in current profile control ability by non zero θ_v beams
(Reactor Parameters A)

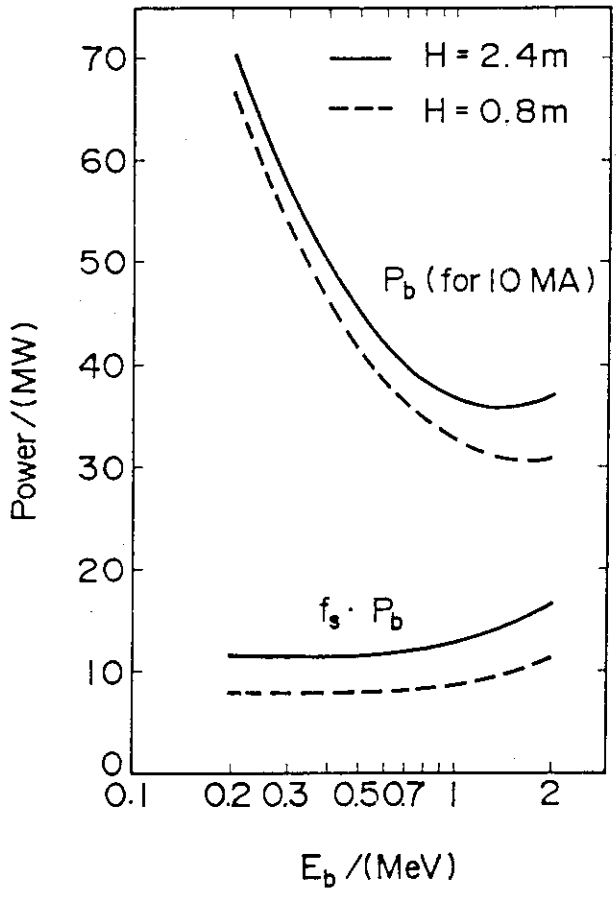

Fig. 18 Beam Power and shinethrough power in a transformer recharge phase
$\bar{n}_e = 0.1 \times 10^{20}$ m^{-3}, $\bar{T}_e = 10$ keV, $I_D = 10$ MA.
Solid lines indicate beam height
H = 2.4 m, and broken lines indicate
H = 0.8 m
(Reactor Parameters A)

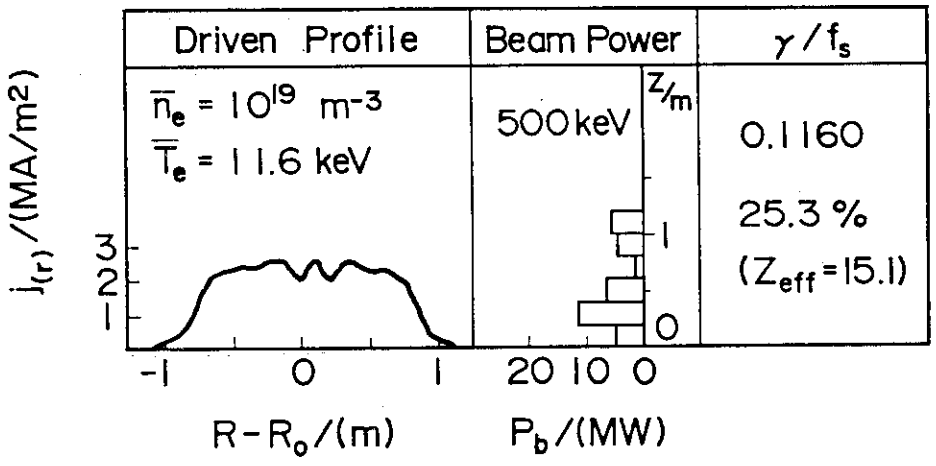

Fig. 19 Driven current profile during transformer recharging $\bar{n}_e = 0.1 \times 10^{20}$ m^{-3}, $\bar{T}_e$ = 11.6 keV, I_D = 12.7 MA (Reactor Parameters A)

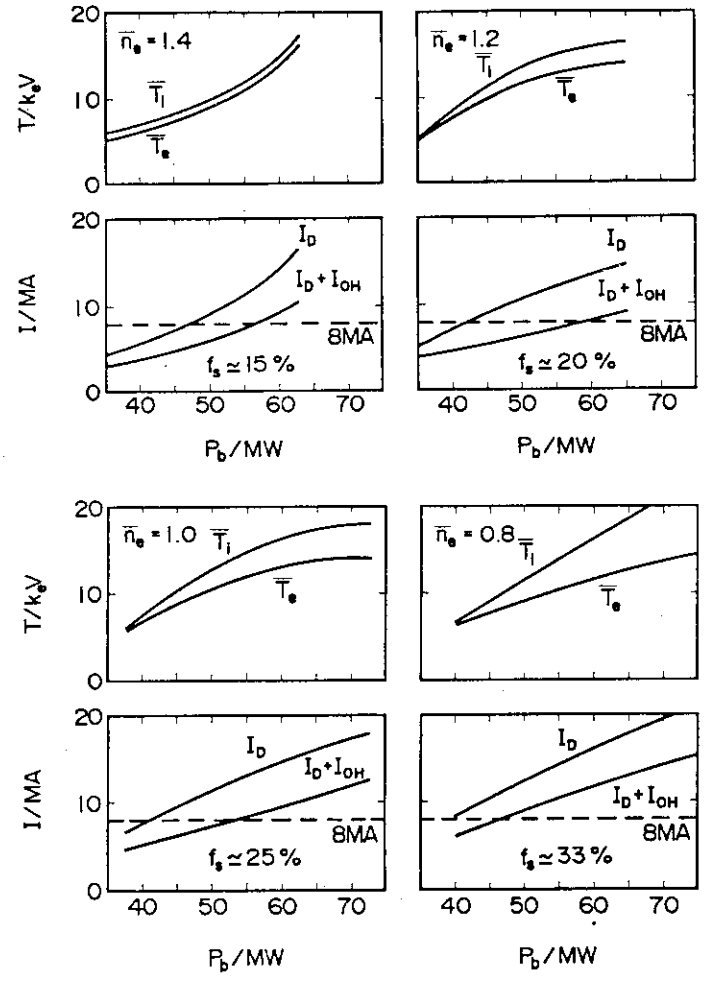

Fig. 20 Parameter scan results for transformer recharge phase. $\bar{n}_e$ = 0.8, 1.0, 1.2 and 1.4 $\times 10^{19}$ m^{-3}, respectively (Reactor Parameters A)

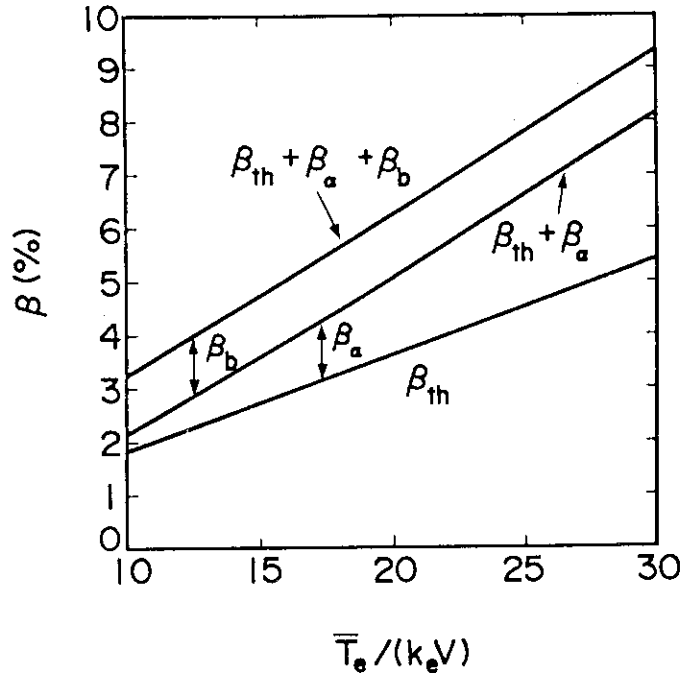

Fig. 21 T_e-dependence of β_b, β_α and β_{th} (Reactor Parameters A)

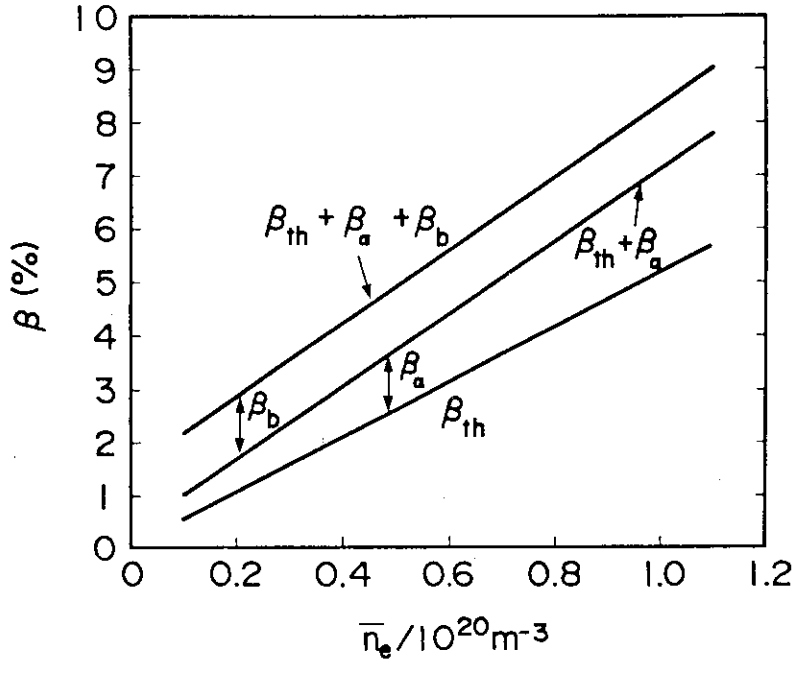

Fig. 22 n_e-dependence of β_b, β_α and β_{th} (Reactor Parameters A)